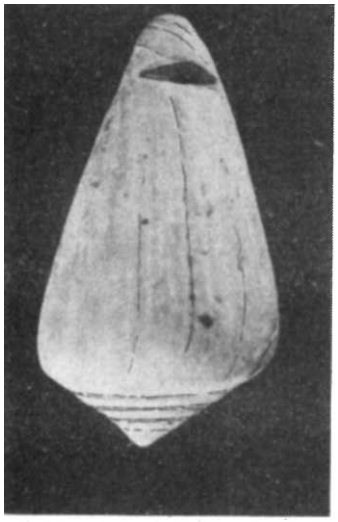

Fig. 3 Shell of a snail (*Conus* sp.) with an intentional aperture at the basal end. Assumed to have been used as bullroarer or pendant.

Fig. 4 Ventral view of the adult distal left thumb phalanx.

piece. Red colouring from a mineral substance was detected on some parts of the weapon, but there is no evidence to suggest that this is a result of painting.

Apart from the boomerang this lowest cultural level contained seven other artefacts made of organic materials. These include: a wedge made from the distal fragment of the antler from a large cervid, with a sharpened working end and decoration consisting of a few parallel arcuate lines (Fig. 2); a pendant or possible bullroarer made of a snail shell (*Conus* sp.) (Fig. 3); a necklace element made of the upper canine of an Arctic fox (*Alopex lagopus*); a perforator; and three bone beads. The assemblage of 30 stone artefacts comprise two flint cores and one of radiolarite, some blades, flakes and tools. Among the tools is an oblique truncated blade with undulating truncation (of Rgani type), a short end-scraper and a large tool of a cleaver type. The remains of a structure which consisted of several large granite and sandstone boulders up to 0.5 m in diameter were also found in this layer. Finally this cultural level also yielded the distal phalanx of an adult left thumb (Fig. 4), which represents the earliest find of human remains in Poland, as well as the bones and teeth of amphibians, reptiles, birds, and mammals, including Arctic lemming (*Dicrostonyx gulielmi*), Norway lemming (*Lemmus lemmus*), souslik (*Spermophilus* sp.), root vole (*Microtus oeconomus*), narrow-skulled vole (*Microtus gregalis*), snow vole (*Microtus nivalis*), pika (*Ochotona* sp.), hare (*Lepus* sp.), wolf (*Canis lupus*), Arctic fox (*Alopex lagopus*), stoat (*Mustela erminea*) and reindeer (*Rangifer tarandus*).

The faunal material from the cultural level containing the boomerang is not homogeneous in origin. The abundant fauna of small vertebrates undoubtedly derive from owl pellets, while some of the larger bones may represent food remains of other animal inhabitants of the cave as well as the bones of animals which died inside the cave. There is relatively little human food debris and this comprises heavily split reindeer bones for the most part, suggesting that the Palaeolithic people living in this cave hunted mainly this ungulate. The whole faunal complex indicates a cold period of the last glaciation when the extensive steppe-tundra covered the cave environs.

In general the artefacts of the lowest cultural level in question can be related to the complex of Central European cultures with backed points, showing traits of the Pavlov culture which is about 23,000 yr BP. The cultural characters of the inventory and the geographical position of the cave suggest that this site might have been of importance in the course of migration of human groups with backed points from today's Moravia and south-western Slovakia north-eastwards to the Don river basin[10].

We thank Dr E. Gleń-Haduch for anthropological expertise on the human skeletal element excavated, Dr M. Pawlikowski for mineralogical investigation of the red colour substance covering the boomerang and Drs J. Cook and A. W. Gentry for valuable comments.

Received 29 Janury; accepted 12 August 1987.

1. Thomas, J. *New Scient.* **99**, 838-843 (1983).
2. Bell, J. *New Scient.* **99**, 839 (1983).
3. Peter, H. *Wesen und Bedeutung des Bumerangs* (Braumüller, Vienna, 1986).
4. Hess, F. *Antiquity* **47**, 303-306 (1973).
5. Schwantes, G. *Deutschlands Urgeschichte* (Quelle and Meyer, Leipzig, 1934).
6. Kriegler, K. *Acta praehist.* **3/4**, 6-13 (1962).
7. Menghin, O. F. A. *Acta praehist.* **3/4**, 14-34 (1962).
8. Kowalski, K. *Jaskinie Polski.* Vol. 3 (Panstwowe Wydawnictwo Naukowe, Warsaw, 1954).
9. Birkenmajer, K. *Przewodnik geologiczny po pieninskim pasie skałkowym* (Wydawnictwa Geologiczne, Warsaw, 1979).
10. Kozłowski, J. K. & Kozłowski, S. K. *Pradzieje Europy od XL do IV tysiaclecia p.n.e.* (Panstwowe Wydawnictwo Naukowe, Warsaw, 1975).

Endstopped neurons in the visual cortex as a substrate for calculating curvature

Allan Dobbins, Steven W. Zucker & Max S. Cynader*

Computer Vision and Robotics Laboratory, McGill Research Centre for Intelligent Machines, McGill University, 3480 University Street, Montréal, Québec H3A 2A7, Canada

Neurons in the visual cortex typically respond selectively to the orientation, and velocity and direction of movement, of moving-bar stimuli. These responses are generally thought to provide information about the orientation and position of lines and edges in the visual field. Some cells are also endstopped, that is selective for bars of specific lengths. Hubel and Wiesel first observed that endstopped hypercomplex cells[1] could respond to curved stimuli and suggested they might be involved in detection of curvature, but the exact relationship between endstopping and curvature has never been determined. We present here a mathematical model relating endstopping to curvature in which the difference in response of two simple cells gives rise to endstopping and varies in proportion to curvature. We also provide physiological evidence that endstopped cells in area 17 of the cat visual cortex are selective for curvature, whereas non-endstopped cells are not, and that some are selective for the sign of curvature. The prevailing view of edge and curve determination is that orientations are selected locally by the class of simple cortical cells[3] and then integrated to form global curves. We have developed a computational theory of orientation selection[4,5] which shows that measurements of orientation obtained by simple cells are not sufficient because there will be strong, incorrect responses from cells whose receptive fields (RFs) span distinct curves (Fig. 1). If estimates of curvature are available, however, these inappropriate responses can be eliminated. Curvature provides the key to structuring the network that underlies our theory and distinguishes it from previous lateral inhibition schemes[6,7].

The defining characteristic of endstopped cells is the presence of inhibitory receptive field (RF) end zones that 'stop' the response of the cell to stimuli which are long enough to intrude into the end zones. Two alternative models of endstopping have been proposed[1,2]: in one, the inhibitory 'endzones' derive from two or more independent cortical afferents with offset RFs; in the other, they derive from a single inhibitory input with a long RF. Both are compatible with the requirement that the endzones

* Departments of Physiology, Biophysics and Psychology, Dalhousie University, Halifax, Nova Scotia B3H 4J1, Canada.

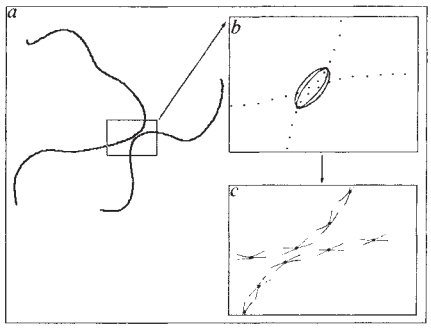

Fig. 1 Illustration of the use of curvature information in orientation selection. *a*, Two distinct curves closely approach each other so that the tangent to a point on one of the curves is colinear with the tangent to a nearby point on the other curve. *b*, This region is schematically expanded. In simulations, a simple cell-like operator centred between the curves and spanning both is strongly activated. This leads to an incorrect representation of the two distinct arcs as a single, unresolved curve. *c*, Each cone-like segment represents bounds on the estimate of curvature at a point. If such estimates were available, for example from the model that we propose, then the incorrect simple cell responses linking the two curves could be eliminated. A network for accomplishing this is described in detail in Parent and Zucker[15].

share the orientation preference of the excitatory centre[1,8]. Current evidence favours inhibition by a single large RF cell[9] for reversible inactivation of layer VI, which contains the long RF cells[10], eliminated or reduced endstopping in layer IV and the superficial layers; there is also anatomical evidence for a layer VI to IV connection[11,12].

With this background, observe that curvature can be defined as the rate of change of the tangent direction along a curve. For straight lines there is no change, whereas for circles the change is constant. Therefore, curvature varies directly with deviation from straightness over a local neighbourhood through which the curve passes.

In our model for estimating curvature, two simple cells estimate the straightness of a contour, one over a small neighbourhood and the other over a larger one, and the difference in their responses, which converge upon an endstopped simple cell (ES), varies with the deviation from straightness, that is, the curvature. Consider two similarly positioned and oriented simple cells with RFs of different size, termed the small and large simple cells. An endstopped simple cell receives excitation from the small cell and inhibition from the large cell, thereby encoding both orientation and curvature information. In symbols, let R_S denote the response of the small simple cell, R_L the response from the large simple cell to a particular contrast pattern at the same position and orientation, $\phi(\cdot)$ a rectifying or clipping function equal to its argument when positive (when excitation sufficiently exceeds inhibition) and zero otherwise, then the end-inhibited simple cell response is given by

$$R_{ES} = \phi(c_S \cdot \phi(R_S) - c_L \cdot \phi(R_L))$$

where c_S and c_L are positive constants that normalize the area difference between the receptive fields (Fig. 4). The non-linear clipping in the model increases the stimulus specificity by preventing a negative value for R_L from being flipped into a positive contribution to R_{ES}, the response of the ES cell. $\phi(\cdot)$ models the inability of spike trains to code negative numbers against a background of low spontaneous activity such as that found in area 17. The simple RFs can have either even or odd symmetry, that is, can be either symmetrical or anti-symmetrical about the central axis and Fig. 2 shows ES models composed of differences of each type.

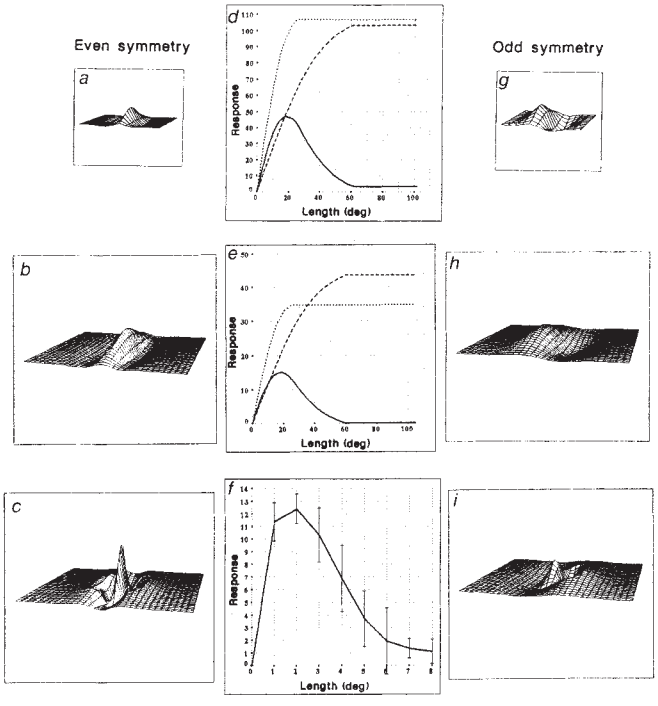

Fig. 2 The endstopped simple (ES) model. Binocular and temporal properties, and their non-linearities, are not incorporated, allowing the retinogeniculo-cortical pathway to be collapsed into a spatial receptive field, so the response of the cell can be modelled as a two-dimensional spatial convolution. Each simple RF may be modelled as a Gabor function or a difference of Gaussians (DOG). *a*, *b*, *c*, (Left column) Representation of the RF profiles of two even-symmetric simple cells and their linear combination. Each simple RF has a Gaussian weighting along the long axis and a DOG in the perpendicular direction. For these two simple RFs, the width ratio of the Gaussians comprising the DOG (σ_{x2}/σ_{x1}) is 2.5. The aspect ratios (σ_y/σ_{x1}) are 4 and 5 for the small and large RFs respectively. The smaller RF is 25 units long and the larger is 61. A linear combination of the two is also shown with weight constants $C_S = 3$ and $C_L = 1$. This graphic representation corresponds to the ES model only when the results of both simple convolutions are positive. (These parameter values are also used in Figure 3*d*.) *d*, *e*, *f* (Middle column), Length responses of even- and odd-symmetry ES models and of an end-stopped neuron respectively. *d*, The response of even-symmetry ES cell model to optimally-oriented bars of different length centered on the RF. The ES-cell model (solid curve) and the component responses of the two simple cells ($C_S \cdot \phi(R_S)$ and $C_L \cdot \phi(R_L)$, the dotted and dashed curves, respectively) were computed for bars 3 units wide with 50 lengths ranging from 2 to 100 units. *e*, The length-response of the odd-symmetry ES cell model (solid, dotted and dashed curves as in *d*). *f*, The actual response to moving bar stimuli of varying length obtained from an end-stopped neuron. *g*, *h*, *i* (Right column), Representation of the RF profiles of two odd-symmetry simple cells and their linear combination.

Methods. Surgery was performed under sodium pentothal anaesthesia with marcaine (a long-lasting local anaesthetic) applied around the surgical wounds. During the experiment, paralysis was maintained with continuous infusion of flaxedil (10 mg kg^{-1} h^{-1}) with anaesthesia by a respirated mixture of 70% N_2O/30% O_2 supplemented with intravenously infused nembutal (1 mg kg^{-1} h^{-1}). The animal was also infused with 5% dextrose in lactated Ringer solution (2 ml h^{-1}). Rectal temperature, end-tidal CO_2 and electrocardiogram were continuously monitored. Neuronal responses were assessed quantitatively by measuring: length tuning using optimally-oriented bar stimuli moving in the preferred direction, line-weighting functions (bars of the preferred orientation flashed throughout the central RF), and curvature-tuning with semi-circular arcs spanning a wide range of radii, moved in the preferred direction and positioned so that the tangent of the curve at mid-arc passes over the central RF parallel to the preferred orientation of the RF. For a more detailed description of our surgical and recording procedures see Ref. 13. *g*, *h*, *i*, The two odd-symmetry simple RFs are described by Gabor functions (a 2-D Gaussian multiplied by a sinusoid). For the small and large simple RFs (*g*, *h*), the aspect ratio (σ_y/σ_x) is 3 and the period ratio (λ/σ_x) is 2, where λ is the period of the sine function. *i*, Shows a linear combination of the two ($C_S = 2.5$ and $C_L = 1$). Again, the non-linear components of the model are omitted.

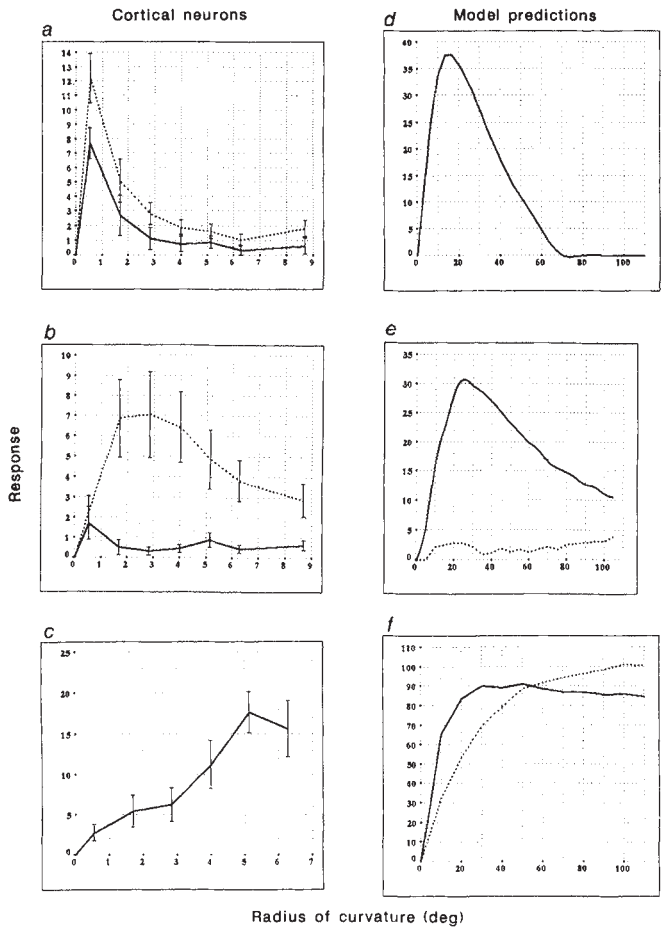

Fig. 3 Experimental (*d, e, f*) and theoretical (*a, b, c*) curvature-response data. Solid and dotted curves correspond to the two signs of curvature in all parts of the figure except *f*. *a, b, c* (Left column), Curvature-response of three area 17 neurons evaluated with semi-circular white arcs projected onto a darker screen. The tangent at mid-arc was parallel to the preferred orientation of the RF and moved in the preferred direction. The curves are based on sample means and standard errors from 16 randomly-interleaved presentations. A cubic spline was used to interpolate smoothly between the points in *a–e*. *a*, The curvature response of the endstopped neuron for which the length response is shown in Fig. 2*f*. The response does not vary with sign of curvature. *b*, Curvature response of an endstopped neuron. *c*, Curvature response of a nonendstopped neurone. *d–f* (Right column), Curvature response of even- and odd-symmetry instances of the model and the component responses of the even model produced by convolving the ES model with semi-circular arcs 3 units wide with different radii, to illustrate the sensitivity of the ES model to curvature. The curves are positioned so that the tangent to the curve at the point on the RF centre is parallel to the long axis of the RF. In each case the model was convolved with 20 curves varying in radius from 5 to 100 units. *d*, Curvature response of the even-symmetry ES model with the parameter values given in Fig. 2. *e*, Curvature response of the odd-symmetry model of Fig. 2 for the two signs of curvature, showing how different combinations of small and large cells give rise to different curvature selectivity and in particular, providing a suggestion for how different responses to the two signs of curvature could arise. *f*, Curvature response of the two simple components of the ES model in *d*, demonstrating how curvature selectivity arises. The non-endstopped neuron (*c*) and non-endstopped simulations (*f*) have a much broader band pass than the endstopped neurons and simulations.

Responses as a function of length for the even- and odd-symmetry ES models and their simple RF components are shown in Fig. 2*d, e*: a typical length response curve obtained in one of our neurophysiological experiments is shown for comparison (Fig. 2*f*). By varying the size of the two receptive fields, within

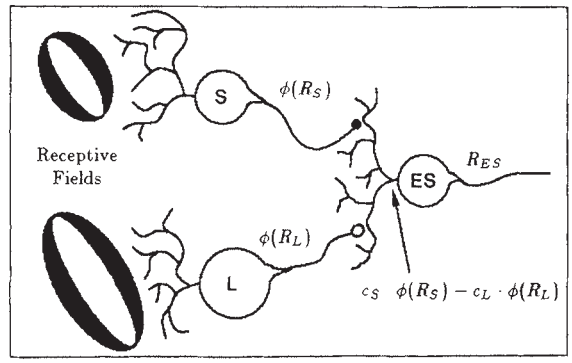

Fig. 4 A schematic model of the endstopped simple circuit. Neurons classified as simple cells with small (S) and large (L) receptive fields provide excitation and inhibition, respectively, to the endstopped simple cell (ES) upon which they converge.

physiological limits, and the weighting constants, it is possible to replicate any of the length-response data found in the literature while preserving position and orientation tuning. Although we shall not consider them further here, various combinations of weights and sizes are necessary to deal with the contrast and width variations that arise in natural images[14].

By analogy with a length-response curve, a curvature-response curve can be obtained by evaluating the model over a series of semi-circular arcs with increasing radius (Fig. 3). Two possibilities arise, one in which the model is composed of even-symmetry simple cells, and one in which they have odd symmetry. Consider the even-symmetry model first. For a stimulus with a low radius of curvature, the curve passes through the excitatory region of the receptive field of the small simple cell but does not pass through enough of the excitatory region of the receptive field of the large simple cell to inhibit it effectively. As the radius of curvature increases, the stimulus becomes increasingly effective in driving the large receptive field and the inhibition increases. Figure 3*d, f* shows the curvature response for the ES model and its even-symmetry components. For the odd-symmetry ES model, the curvature-response depends on the sign of curvature (Fig. 3*e*). For one sign of curvature, a curved stimulus excites the small RF but curves into the antagonistic region of the large RF, reducing its response and hence its inhibitory contribution to the ES cell. A similarly curved stimulus of the opposite sign passes through only the excitatory region of the large RF, allowing effective inhibition. For both signs of curvature, as the radius of curvature increases, inhibition becomes increasingly effective.

These computational results encouraged us to seek evidence for curvature-selective neurons in area 17 in the visual cortex of the cat. We will describe a cell as curvature-selective, if it responds strongly over only a limited range of curvatures when stimulated with a continuous arc falling within a range of positions and orientations at the centre of the RF. The curvature response of both endstopped and non-endstopped cells was examined to determine if curvature-selectivity is systematically related to endstopping. Cells were qualitatively characterized using a hand projector and then examined quantitatively using computer-controlled optics.

All of the fifteen endstopped neurons, both simple and complex, examined carefully so far exhibit the predicted peaked curvature response (Fig. 3*a, b*) whereas non-endstopped neurons exhibit a different, non-peaked response (Fig. 3*c*). The neuron of Fig. 3*a* displays similar curvature tuning for both signs of curvature, qualitatively resembling the even-symmetry model, whereas the one in Fig. 3*b* has virtually no response for one direction of curvature, similar to the odd-symmetry model. More than a third of the neurons exhibited significantly stronger responses to one direction of curvature than to the other, the cell in Fig. 3*b* being one of the most striking examples. Although

most endstopped cells are directionally selective, we tested curvature response in both the preferred and null (opposite) directions of motion for some of the less directionally sensitive units. The results indicate similar curvature selectivity for both directions of motion.

In comparing the single unit results to the predictions of the ES model, note that layer VI contains complex RF types as well as simple, and they may also contribute to the generation of end inhibition and curvature-selective responses. Even so, an asymmetrical contribution from the large RF cell, whether of spatial or temporal origin, is required to generate responses selective for sign of curvature. Because experiments to determine the basis of this selectivity have not yet been performed, inhibition from a large, odd-symmetry inhibitory RF (Figs 2 and 3) must be considered as only one of the possible mechanisms.

Obtaining straightness (tangent) and curvature estimates from a difference of two first-stage responses has two advantages: anatomically, only vertical connections within a cortical column are required, and numerically, there is greater noise immunity in a first-difference operation than in repeated-difference operations.

Endstopping is usually thought to be related to length or end-point detection. We provide evidence for an alternative, that orientation-selective end inhibition allows the calculation of coarse-curvature estimates. Such estimates facilitate the process of orientation selection, and could be important in shape representation. As there are far more curves than end points in natural images, this proposal has a certain ecological plausibility.

We thank L. Iverson for programming support. Research was supported by grants from DREA, MRC and NSERC (S.W.Z., M.S.C.). S.W.Z. and M.S.C. are Senior Fellows of the Canadian Institute of Advanced Research.

Received 26 May; accepted 7 August 1987.

1. Hubel, D. H. & Wiesel, T. N. *J. Neurophysiol.* **28**, 229–289 (1965).
2. Dreher, B. *Invest. Opthalmol.* **11**, 355–356 (1972).
3. Hubel, D. H. & Wiesel, T. N. *J. Physiol.* **160**, 106–154 (1962).
4. Zucker, S. W. *Comp. Vis. Gr. Im. Proc.* 74–103 (1985).
5. Zucker, S. W. *Behav. Res. Meth., Instr. Comp.* **18**, 608–617 (1986).
6. Blakemore, C., Carpenter, R. & Georgeson, M. *Nature* **228**, 37–39 (1970).
7. Carpenter, R. & Blakemore, C. *Expl Brain Res.* **18**, 287–303 (1973).
8. Orban, G. A., Kato, H. & Bishop, P. O. *J. Neurophysiol.* **42**, 833–849 (1979).
9. Bolz, J. & Gilbert, C. D. *Nature* **320**, 362–365 (1986).
10. Gilbert, C. D. *J. Physiol.* **268**, 391–421 (1977).
11. McGuire, B. A., Hornung, J-P., Gilbert, C. D. & Wiesel, T. N. *J. Neurosci.* **4**, 3021–3033 (1984).
12. Wiesel, T. N. & Gilbert, C. D. *Quart. J. exp. Physiol.* **68**, 525–543 (1983).
13. Baker, C. L. & Cynader, M. S. *J. Neurophysiol.* **55**, 1136–1152 (1986).
14. Dobbins, A. *thesis*, McGill University, 1987.
15. Parent, P. & Zucker, S. W. *IEEE Trans. PAMI* (in the press).

Kindling stimulation induces c-*fos* protein(s) in granule cells of the rat dentate gyrus

M. Dragunow & H. A. Robertson

Department of Pharmacology, Faculty of Medicine,
Dalhousie University, Halifax, Nova Scotia B3H 4H7, Canada

Alterations in neuronal gene expression have been proposed to account for permanent changes in brain function such as learning and memory[1–4]. In particular, it has been suggested that proto-oncogenes such as c-*fos* (ref. 5) may be rapidly induced in conditions that lead to neuronal plasticity and evoke permanent changes in the expression of effector genes[1]. Concentrations of the c-*fos* proto-oncogene increase rapidly following depolarization-induced calcium influx in non-dividing neuronally differentiated PC 12 cells[2,3]. Recently, the presence and induction of c-*fos* in the adult brain and spinal cord has been observed[6–8]. Here we report that electrically-induced seizure activity, which leads to a permanent increase in the response of the brain to future seizures (kindling[9]), rapidly and transiently increases c-*fos* protein-like immunoreactivity in the nuclei of granule cells in the rat dentate gyrus. These results suggest that c-*fos* protein is present within the nuclei of adult mammalian neurons, and could be involved in plastic changes in the nervous system associated with seizure activity.

To study the effects of kindling stimulation on the production of c-*fos* protein(s), 40 adult male Sprague-Dawley rats were anaesthetized with barbiturate and bipolar stainless steel electrodes were implanted unilaterally into the dorsal hippocampus as previously described[10]. At least one week later, rats were electrically stimulated with high frequency trains (kindling stimuli: 500 μA, 100 Hz, 0.5 ms/half-wave diphasic pulses for 2 s) which produced brief partial hippocampal seizures, comprising an initial burst of high frequency and amplitude spiking lasting from 10–20 s, followed by a post-ictal electroencephalogram silence that was terminated by a second bout of afterdischarge lasting from 10–30 s. At various times after the spontaneous termination of these partial hippocampal seizures, rats were anaesthetized with barbiturate, and perfused and fixed for c-*fos* protein immunohistochemistry as previously described[6].

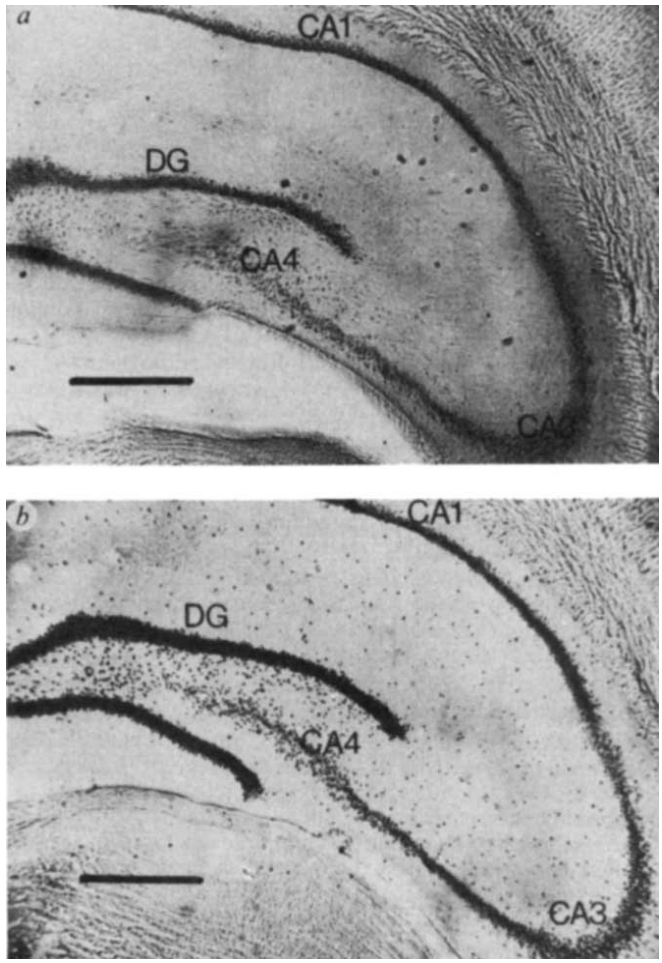

Fig. 1 *a*, Photomicrograph of rat hippocampal formation (areas CA1, CA3, and CA4) and dentate gyrus (DG) from an electrode implanted unstimulated rat. *b*, Photomicrograph of rat hippocampal formation and dentate gyrus fixed 30 min following a hippocampal seizure. Note the intense immunoreactivity in dentate granule cells and the increase in immunostaining in the pyramidal cells of areas CA1, CA3 and CA4. Antiserum was diluted 1 in 1,000 (Scale bar, 0.5 mm).